INTEGRATED STRUCUTURAL MONITORING OF COMPOSITE MATERIALS VIA DISTRIBUTED OPTICAL SENSOR

Jung-Ting Tsai[1,3] , Joshua S. Dustin[3] , and Jan-Anders Mansson[2,3]
[1]School of Materials Engineering, Purdue University
[2]School of Materials Engineering and School of Chemical Engineering, Purdue University
[3]Composites Manufacturing & Simulation Center (CMSC)

Abstract

Measuring the strain history in pre-impregnated thermoset composites during the curing process provides valuable data for manufacturing specification development, quality control, diagnostics of dimensional stability, and validation of cure models. Unlike traditional fiber-brag grating based methods, Distributed Optical Sensors (DOS) provide information along the entire optical distance (optical path length) of the sensor embedded in the laminate for strain measurement. This study's unique contribution to the field is the coupling of the optical sensor monitoring of composite cure strain with models of the cure kinetics, viscosity, and glass transition temperature of the thermoset matrix. Coupling the strain measurements to the material models facilitates coherent comparisons between strain sensor output and thermoset material behavior during the cure process rather than making suppositions of material behavior based on the strain measurement alone. In this research, two laminate types were manufactured with an embedded optical sensor from IM7/5320-1 prepreg tape; a $[0]_{20}$ unidirectional (UD) laminate and a 50/40/10 (%0°/%±45°/%90°) structural laminate (SL) with the optical sensor routed along three different ply interfaces including [0°/0°], [45°/90°], and [0°/45°]. The internal residual strain developed during each stage of the thermal cure cycle is examined, including after cooling. Results show that the local strain has variable magnitude which depends on the ply configuration. The laminate micro-structure was also investigated by optical microscopy for selected cross-sections to provide the resin pocket geometry created by different optical sensor placement in the laminates. Lastly, a Micromechanics-Base approach was used to calculate the chemical shrinkage and the residual strain in the UD laminate during curing and compared with the measured results from the DOS to further validate the strain measurements.

Keywords: optical sensors, embedded sensor, distributed strain, out-of-autoclave prepreg, cure behavior, residual/ internal strain, and composite material

Background

Optical fiber sensors for structural monitoring are found in the aerospace, automotive, infrastructure, pressure vessels, sports and wind turbine industries [1, 2]. A natural use of these sensors in laminated composite structures involves embedding optical fibers in structural composite materials during processing and cure, which provides a straightforward method to monitor the curing process and quantify effects such as cure shrinkage and thermal residual deformation. Several review papers have previously discussed the application of optical sensors in structural materials monitoring [3-5] where most studies have focused on Fiber Brag Grating (FBG) to monitor the curing shrinkage and stiffness change in the composite plies [6, 7]. In FBG, strain measurement is limited to only the grating location in the optical sensor, so the spatial resolution of these sensors is quite restricted. There can be multiple gratings in an optical sensor, but the process for adding these gratings is expensive, thus limiting the use in most industrial applications. Furthermore, most of the studies of process monitoring involving FBG sensors lack

the theoretical analysis of cure history dependent strains to validate strain measurements during cure so it is difficult to isolate measurement artifacts from actual experimentally observed phenomena. The detailed high-resolution data obtained experimentally from a Distributed Optical Sensor (DOS) requires the complementary theoretical analysis to interpret/understand the local variability of sensor readings, as the coherent interpretation of sensor readings is imperative to improve the strain measurements. Without recognizing the epoxy curing mechanism producing the strain, many experimental factors may be neglect without recognition of the end user.

Previously, Montanini and D'Acquisto [8] used an FBG system to observe the temperature and strain changes in a glass fiber/epoxy system. They showed by using an optical sensor that the reflection of a wave varies under different temperatures and the temperature can be different between the layers. Sanchez et. al [9] used a DOS to monitor resin infusion, the in-situ strain development, and changes in resin viscosity, but the curing mechanisms were not explained extensively from the DOS readings. In discussing the residual strain, the authors have not explained the fluctuation of the local strain reported by the optical sensor. Arhant et. al [10] monitored the curing mechanism during a hot press cycle. Meadows et. al [11] monitored the strains in an adhesive layer in composite joint specimens with DOS. Notwithstanding, the use of DOS to monitor the curing mechanisms has not been thoroughly studied. Therefore, the objective of this research is to interpret the results of curing behaviors from the DOS.

DOS sensors are classified by the techniques used to analyze and reduce the optical data, including Rayleigh scattering, Raman scattering, and Brillouin scattering. Rayleigh scattering corresponds to the strongest intensity range among all three and unlike the inelastic Raman and Brillouin scattering, is an elastic scattering that statically fluctuates along the distance. Elastic scattering produces a linear output from a proportional input power, giving the advantage of detecting the deformation of heterogeneous materials since the proportional response is easier to interpret [5]. Traditionally, Optical Time Domain Reflectometry (OTDR) has been employed to acquire and analyze the data from the scattering mechanisms in the telecom field. OTDR technology is limited by a spatial resolution of 0.1 to 1 m, which produces the corresponding attenuation of the output wavelengths. The uncertainty of measurements and low resolution inherent to OTDR does not make it a suitable choice for the health monitoring of composite structures. Optical Frequency Domain Reflectometry (OFDR) was developed to overcome this spatial resolution limitations of OTDR. OFDR's high spatial resolution of 1 micrometer allows the sensor to be more accurate during monitoring. Distributed optical sensing relies on the detection of the Rayleigh scattering using OFDR, which allows a more efficient and accurate measurement for strain and temperature. Through the use of Rayleigh scattering and OFDR, DOS provides exciting advantages in the area of stain measurement for composite structures including high spatial resolution, easy integration into composite structure, low-cost sensors made of commercially available glass fiber, high measurement sensitivity, and simultaneous strain measurement along the entire sensor length [12-16].

The DOS fiber sensors are small, lightweight, resistant to electromagnetic interference, and can be embedded inside or attached to the surface of any material. Figure 1 (a) shows a cross section of an optical fiber sensor, which consists of an inner-core, cladding, and protective coating. The inner-core and cladding have different optical reflection coefficients to prevent wave refraction which causes signal attenuation. The coating increases the flexibility of the sensor, allowing it to conform to complex curvatures. Distributed Optical Sensors (DOS) have no grating, instead they use the internal flaws in the sensor material formed during production to create measuring reference points along the continuous distance of the fiber. Figure 1 (b) schematically shows the distribution of defects along the length of the optical fiber in undeformed and deformed configurations [12]. The defects act as distributed strain gauges which can experience different

local deformations, such as ($\Lambda_1 - \Lambda_0$) shown in Figure 1 (b). A local deformation leads to a shift in an optical frequency spectrum registered by OFDR.

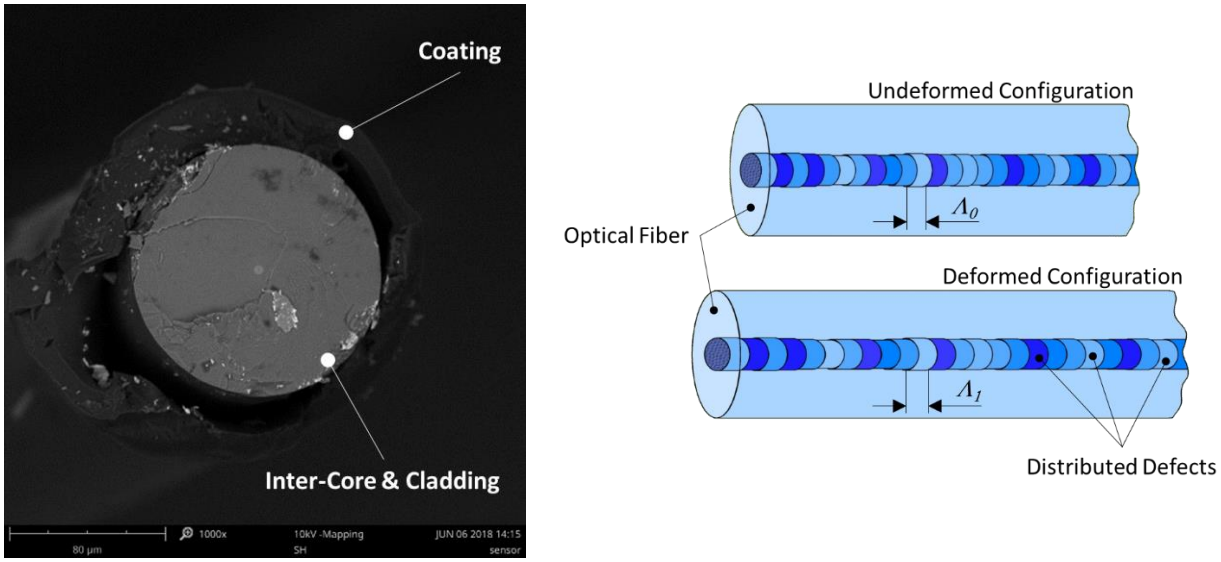

(a) *(b)*

Figure 1 (a) The DOS cross-section; (b) The DOS stretched mechanism

Modeling of a Cure-Induced Deformation in a Unidirectional (UD) Laminate

During the manufacturing thermal cycle, a laminate undergoes deformations caused by the cure and thermal shrinkage of the resin. To observe the cure-induced strains, the ε_{22} strain within a UD laminate is tracked and the cure shrinkage and thermal expansion components are isolated through analysis. The analysis of the transverse strain due to cure shrinkage, $\Delta\varepsilon_{22}(\Delta\xi)$, and thermal expansion, $\Delta\varepsilon_{22}(\Delta T)$, resulting from the advancement of the degree of cure, $\Delta\xi$, and the temperature change, ΔT, is outlined in the following.

Unconstrained cure and thermal shrinkage strain changes in a UD laminate is calculated using equation (1)

$$\begin{Bmatrix}\Delta\varepsilon_{11}\\ \Delta\varepsilon_{22}\\ \Delta\varepsilon_{33}\end{Bmatrix} = \begin{Bmatrix}\alpha_{11}\Delta T - \beta_{11}\Delta\xi\\ \alpha_{22}\Delta T - \beta_{22}\Delta\xi\\ \alpha_{33}\Delta T - \beta_{33}\Delta\xi\end{Bmatrix} \quad (1)$$

with $\varepsilon_{23} = \varepsilon_{13} = \varepsilon_{12} = 0$ and where $\alpha_{11}, \alpha_{22}, \alpha_{33}$ are the lamina effective coefficients of thermal expansion (CTE) and $\beta_{11}, \beta_{22}, \beta_{33}$ are the lamina effective coefficients of chemical (cure) shrinkage.

Schapery's theory [17] was used to obtain the homogenized (effective) CTE and chemical shrinkage coefficients of a lamina from the fiber and resin properties. The expression for the CTE in the longitudinal direction, α_{11} and the transverse direction $\alpha_{22}, and\ \alpha_{33}$ are shown in equations (2) and (3).

$$\alpha_{11} = \frac{\alpha_{1f} E_{1f} f_f + \alpha_m E_m f_m}{E_{1f} f_f + E_m f_m} \quad (2)$$

$$\alpha_{22} = \alpha_{33} = \left(\alpha_{2f} + v_{12f}\alpha_{1f}\right) f_f + (1 + V_m)\alpha_m f_m - V_{12}\alpha_{11} \quad (3)$$

where the subscript f and m denote fiber and matrix; f_f and the f_m are the fiber and the matrix volume fractions; $E_{1f}$and E_m are the longitudinal direction of fiber's modulus and the modulus of the epoxy; and v_{12} is the fiber Poisson's ratio.

Here, it is assumed that the epoxy modulus $E_m(T)$ changes as a function of temperature T [18], as given by equation (4):

$$E_m(T) = -6.58 \cdot T(^{\circ}C) + 3701 \quad (4)$$

The chemical shrinkage equations are derived using the same methods from equation (2) and equation (6) which is expressed as (5) in the longitudinal direction to fiber and (6) as the transverse direction:

$$\beta_{11} = \frac{\beta_m E_m f_m}{E_{1f} f_f + E_m f_m} \quad (5)$$

$$\beta_{22} = \beta_{33} = (1 + V_m)\beta_m f_m - V_{12}\beta_{11} \quad (6)$$

The cure kinetics model for the resin was adopted from Cole, Hechler [19] and Kamal and Sourour [20], and given in equation (7):

$$\frac{d\xi}{dt} = K_1 {\xi_0}^{m_1} * (1 - \xi_0)^{n_1} + \frac{K_2 {\xi_0}^{m_2} * (1 - \xi_0)^{n_2}}{1 + exp(D(\xi_0 - (\xi_{c0} + \xi_{cT})))} \quad (7)$$

where ξ the degree of cure, t is the time, m_1, m_2, n_1, and n_2 are the first and second exponential constants, ξ_{c0} the critical degree of cure at absolute zero, and ξ_{cT} degree of cure with increase temperature, and D is the diffusion constant. K_1 and K_2 are the material dependent.

The DiBenedetto [21] Glass transition model for the resin was used, as given in equation (8):

$$\frac{T_g - T_{g0}}{T_{g\infty} - T_{g0}} = \frac{\lambda \xi}{1 - (1 - \lambda)\xi} \quad (8)$$

where T_{g0} is the glass transition temperature of the uncured resin, $T_{g\infty}$ the glass transition temperature of cured resin, λ is constant.

Values for the constants used in all models are provided in the appendix.

Manufacturing of Composite Material Specimens with Distributed Optical Sensor

Figure 2 (a) and (b) shows the placement of the DOS sensor in the unidirectional and structural laminates. In the unidirectional laminate, the sections of the sensor were aligned with both the 0 and 90 degree directions, while in the structural laminate the sensor was embedded between [90°/45°], [0°/0], and [45°/0°] plies all along the 0 degree direction. A small opening was slit in each ply parallel to the fibers so that that the DOS can route to the next layer. The

dimensions of the structural laminate [45°/0°/0°/-45°/90°/45°/0°/0°/-45°/0°]s were 12'' x 2'' and the dimensions of unidirectional laminate $[0]_{20}$ were 5'' x 5''. After layup and insertion of the DOS sensor, the laminates were debulked for 30 minutes to ensure that no air was trapped within the laminate. Also, two k-type thermocouples were installed: one attached close with the DOS in the oven chamber and the other is embedded within the laminate. Strain data was recorded using the OFDR via an interrogator. The acquisition rate was set at 23.8 Hz with gage length at 1.3mm. This system can monitor the strain with the range of +/- 10,000 micro-strains with the accuracy of +/- 25 micro-strains.

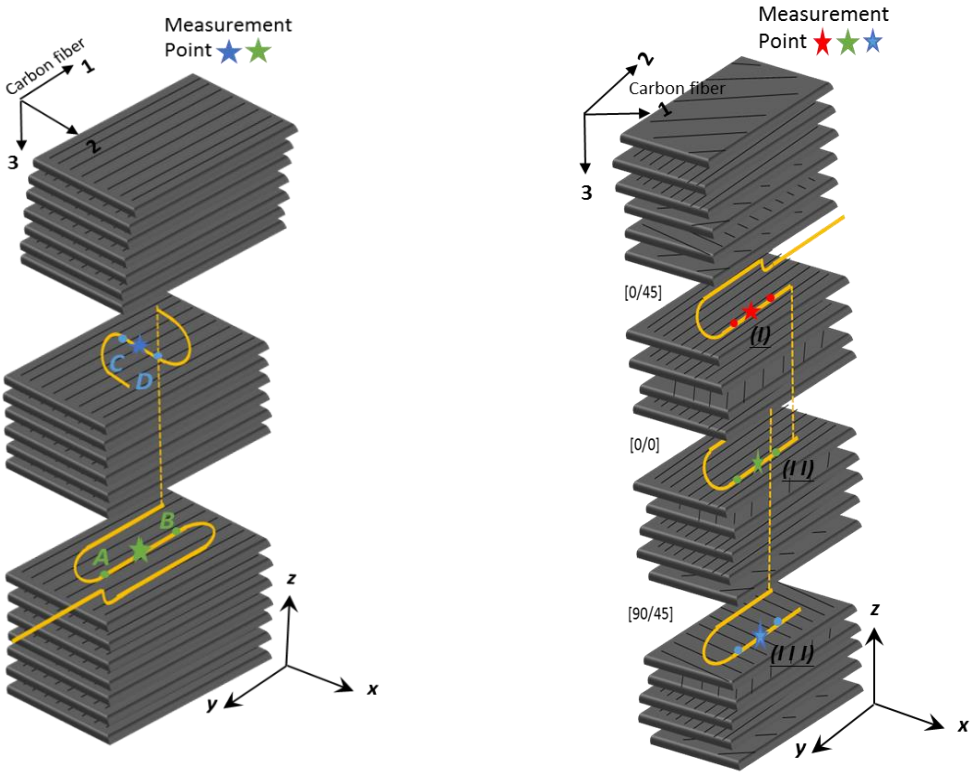

(a) Unidirectional Laminate (UD) *(b) Structural Laminate (SL)*

Figure 2 Schematics of embedment of the DOS into the laminates

Consider point A and point B shown in Figure 3. Both the laminate and the DOS expand or contract during temperature changes. Accurate measurement of the laminate strain requires accounting for the DOS sensor thermal expansion. Because the CTE of the DOS and the laminate are in general different, the total strain reported by the DOS has both thermal and mechanical components. Thermal effects can be separated from the total strain acquired by the DOS using the following equation:

$$\varepsilon_{Laminate} = \varepsilon_{DOS} - (\alpha_{DOS} * \Delta T) \quad (9)$$

where $\varepsilon_{Laminate}$ is the laminate strain, ε_{DOS} is the reading from the DOS, α_{DOS} is the thermal expansion of the DOS, and ΔT is the temperature change from room temperature.

The DOS comes with a polyimide coating. The polyimide CTE is temperature dependent, therefore the CTE of the DOS is measured as $\alpha_{DOS} \sim (7.27 \ldots 9.93) \mu\varepsilon/\,^{\circ}\mathrm{C}$ over the temperature range of the cure cycle. In the local regions of the laminate, ΔT various from ply to ply. The variability of heat conduction between the tool and the laminate results in the heat lag, which causes strain drops/spikes during the temperature ramping.

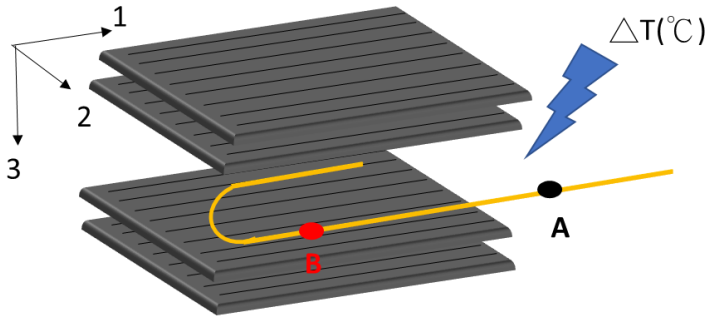

Figure 3 The schematic of DOS inside and outside the laminate

Sensor Location Compared to the Laminate Microstructure

A cross sectional view in Figure 4 shows the embedded sensor positioned along the [0°/45°], [0°/0°], and [90°/45°] interfaces of a structural laminate. Resin pockets are developed around the sensor, and the shape of a pocket and position of a sensor relative to the interface depend on the local stacking sequence of the laminate. The DOS sinks into the 0-degree ply in the [0°/45°]-interface but stays in-between the 0-degree plies in the [0°/0°]-interface. A large elliptical shaped resin pocket is developed around the DOS in the [45°/90°] interface while the sensor itself remains in-between the adjacent plies. In the [0°/0°]-interface, the DOS experiences the most contact with the fibers, thus it is expected that the DOS provides a more constant strain signal from the carbon fiber expansion and contraction.

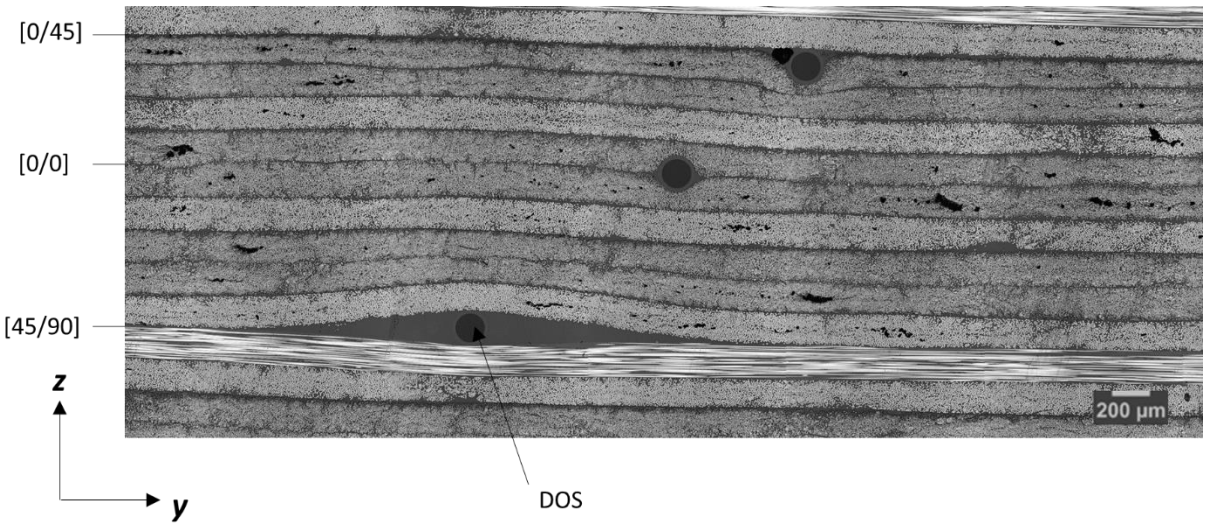

Figure 4 The microscopy of the laminate interface (From the top to the bottom: sensor embedded between [0°/45°], [0°/0°], and [90°/45°])

Distributed Sensing of Cure-Induced Strains in a Composite Laminate

Cure monitoring in a UD Laminate

Figure 5 (a) reports the distribution of the DOS measured axial strain along the segment A-B, shown in Figure 2(a), over the entire time-temperature history. The DOS measured axial strain, ε, along the segment A-B corresponds to the axial strain, ε_{11}, of the UD laminate, as this segment of the sensor is aligned with the laminate fiber direction. It can be observed that strain does not vary substantially along the sensor length, providing a fairly consistent measurement at all times. Figure 5 (b) shows the correlation between the strain and the degree of cure, glass transition temperature, and temperature-time history at a single point (location of the point shown in Figure 2(a)). The temperature profile was input into the cure kinetic equation (7) and glass transition temperature equation (8) to obtain the corresponding curves. The UD laminate has a near zero CTE and high modulus in the axial direction, as these properties are governed by the carbon fiber. Therefore, when the DOS is laid in parallel to the fiber direction of unidirectional plies, the axial strain reading shows very little strain variation. Although there are some drops of strain at the three regions of heat ramp, this is because of the heat lag between the material and the DOS which causes the heat insulation. After passing the gelation and vitrification points, the strain readings remain consistent. During the cool down stage, an increase in strain occurs which is attributed to the slightly-negative axial CTE of the carbon fiber.

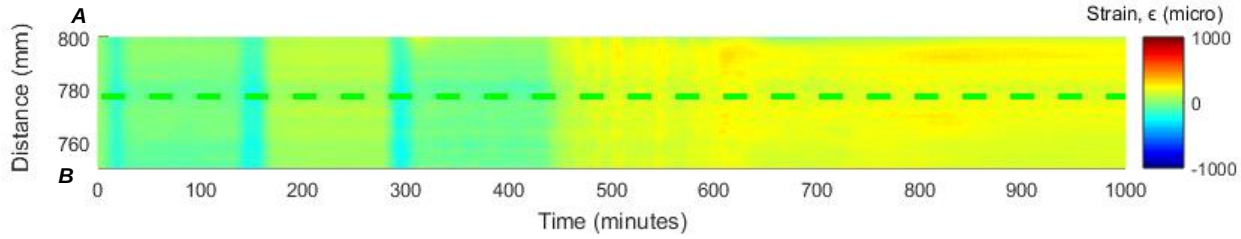

(a)

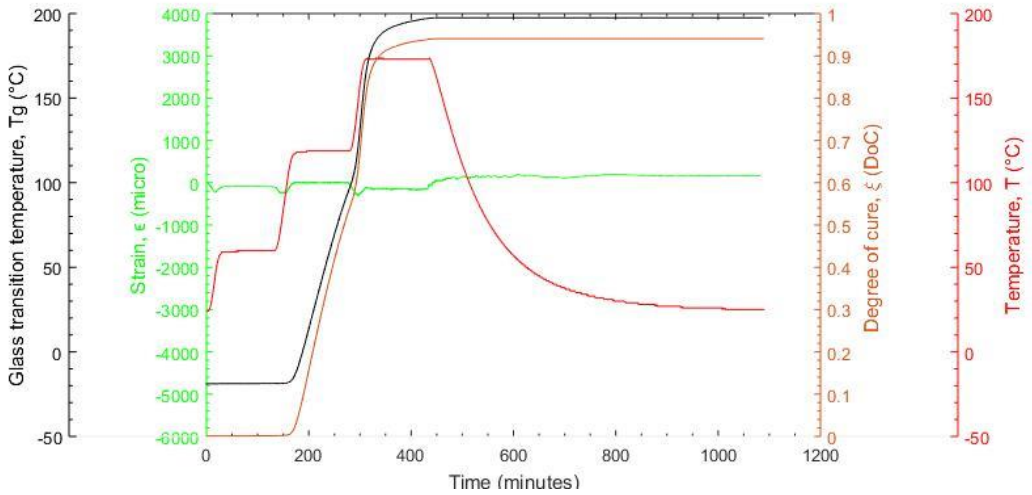

(b)

Figure 5 (a) Strain mapping at section A-B (b) Comparison of Tg, ε_{11}, DoC, and thermal history at UD Laminate

Figure 6 (a) represents the DOS axial strain along the segment C-D, shown in Figure 2(a), over the entire time-temperature history. The DOS measured axial strain, ε, along the segment C-D corresponds to the transverse strain, ε_{22}, of the UD laminate, as this segment of the sensor is perpendicular to the laminate fiber direction. It can be observed that the strain varies substantially during the thermal history. Figure 6 (b) shows the correlation between the UD laminate transverse strain (ε_{22}) and the degree of cure, glass transition temperature, and temperature-time history.

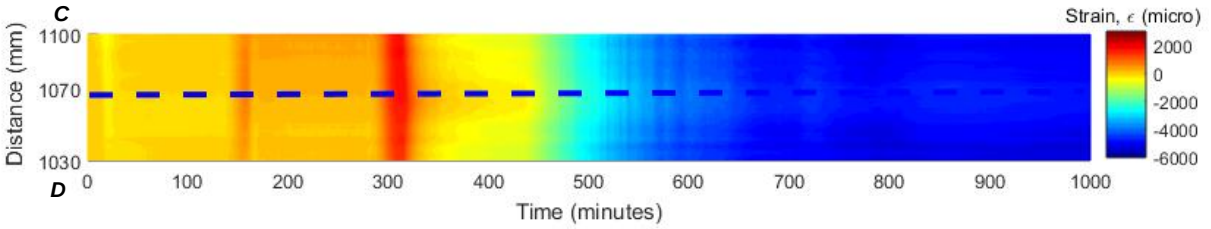

(a)

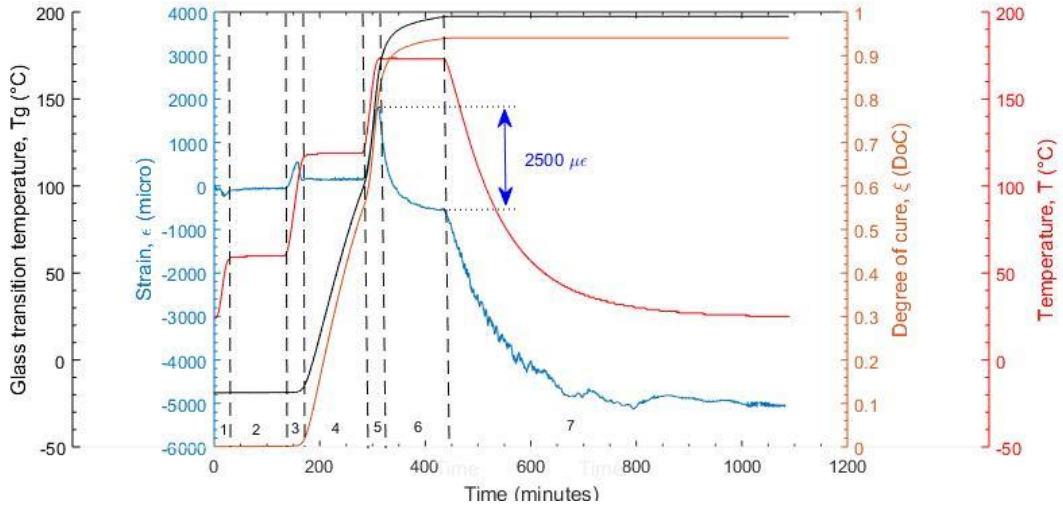

(b)

Figure 6 (a) Strain mapping at section C-D (b) Comparison of Tg, ε_{22}, DoC, and thermal history at UD Laminate

The thermal history consists of seven stages and the strain evolution is analyzed in every stage (Figure 6 (b)). During the first and second stages (first ramp and hold stages), the sensor reports effectively no strain, because of the low viscosity of epoxy when the DOS is not attached to the laminate material. At the third stage (second ramp), small increase in strain was observed because of the thermal expansion of the laminate in the transverse direction. There are two strain spikes at stage one and stage three. As mentioned above, this is due to the heat lag between the laminate and the DOS. At the fourth stage (second hold), the gel point is achieved when the degree of cure reaches approximately 0.55, after that point, the epoxy begins to cross-link. However, the DOS at this stage may not be fully attached to the laminate. Therefore, the strain reading does not change. At the fifth stage (final ramp), the thermal expansion of epoxy and carbon fiber produce the increased strain which dominates the chemical shrinkage (compression) reported by the sensor. Moving on to the sixth stage (the final hold stage); the temperature at this stage passes the vitrification point, and the ongoing chemical shrinkage is captured by the DOS (DoC:0.78). Hence, at the peak temperature, the strain decreases asymptotically, decreasing

approximately -2500 $\mu\varepsilon$ from the peak value. At the final stage, the stain fluctuates at the beginning of cooling. Some researchers have observed similar results during cooling [9, 22]. Some mechanisms which may contribute to the observed strain oscillation during cooling could be related to the increase in epoxy modulus with reduced temperature or tool-part interactions during cooling due to CTE mismatch. The exact cause of the oscillation is still unknown and will be the subject of future study. However, after cooling to room temperature, the residual strain is consistent (approximately -5000 $\mu\varepsilon$).

Cure monitoring in a 50/40/10 (%0°/%±45°/%90°) SL

Figure 7 shows the DOS axial strain along the three selected paths (I,II, and III), shown in Figure 2(b), over the entire time-temperature history. The DOS axial strain, ε, along the three selected paths corresponds to the axial strain, ε_{xx}, of the SL, as this segment of the sensor is parallel to the laminate global x-direction. The strain fluctuations along the sensor length are caused by the locally variable laminate microstructure, such as fiber volume fraction variation, voids, and resin pockets (see Figure 4). Overall, the strain level in the SL is in the range of ~ (-300…200) $\mu\varepsilon$ and is low as compared to the transverse strains in a UD. This is because the high percentage of plies with the fiber direction aligned with the sensor, and the individual plies with different orientations constrain each other's deformation, from both chemical and thermal shrinkage during the cure cycle.

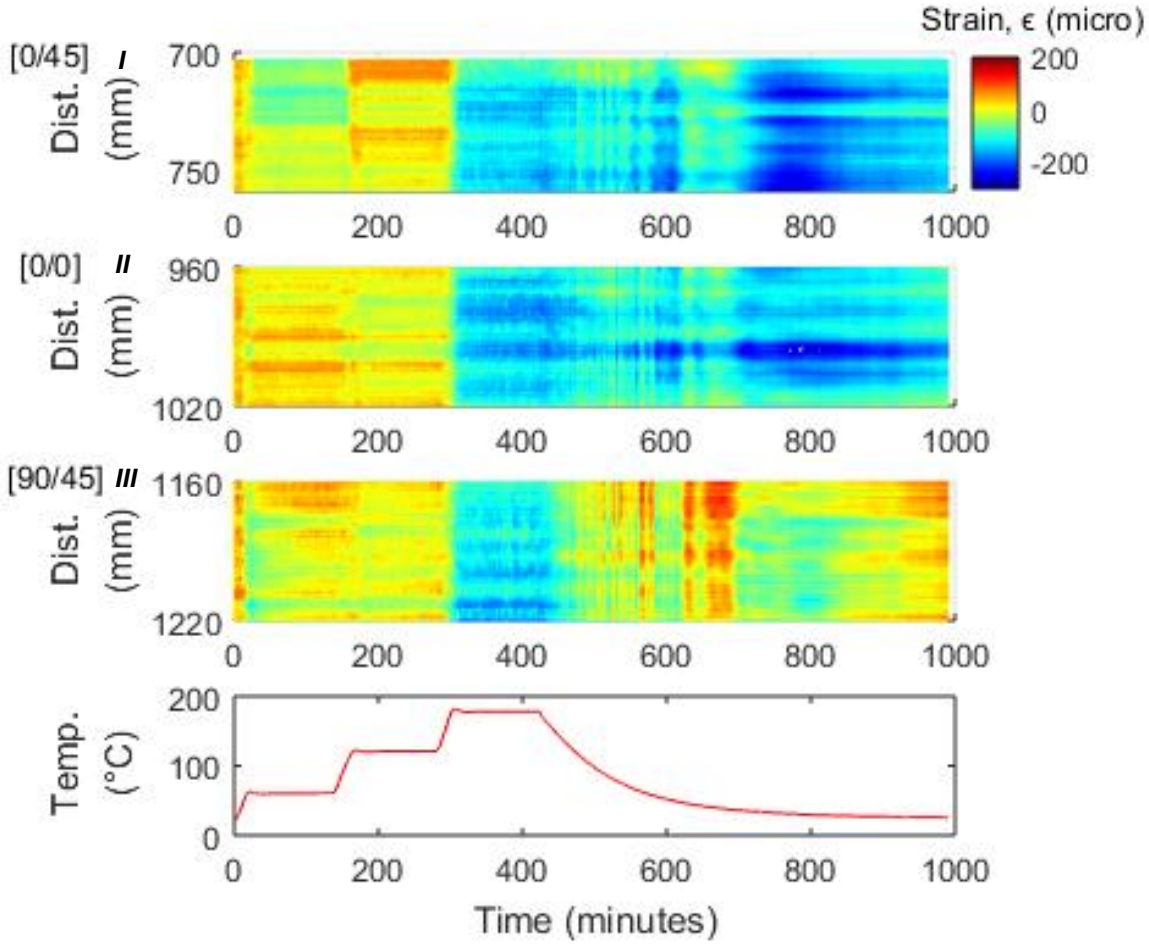

Figure 7 Mapping three selected path at [0°/45°], [0°/0°], and [90°/45°] at SL

Distributed Sensing of Residual Strain in a Composite Laminate

Residual strain monitoring UD Laminate

Figure 8 (a) shows the DOS measured axial strain along the segment C-D in the UD laminate, which is perpendicular to the fiber direction as shown in Figure 2(a), during the cool-down stage. The DOS strain readings correspond to the laminate transverse thermal-residual strain, ε_{22}. The strain fluctuates substantially along the segment C-D length at a given time instance, being in the range ~(-5200…-4700) $\mu\varepsilon$ as shown in Figure 8 (a). One of the sources of local strain variability along the sensor length is the inevitable inaccuracy of sensor alignment with the lamina principal directions. To highlight this effect, an XRD probe was used to scan the DOS embedded in the laminate and determine the DOS orientation in relation to the principal fiber direction. As Figure 8 (b) shows, the DOS is not exactly parallel to the fiber direction after processing. More investigation is needed to proceed on calculating the strain at different DOS local orientations from the experimental measurements.

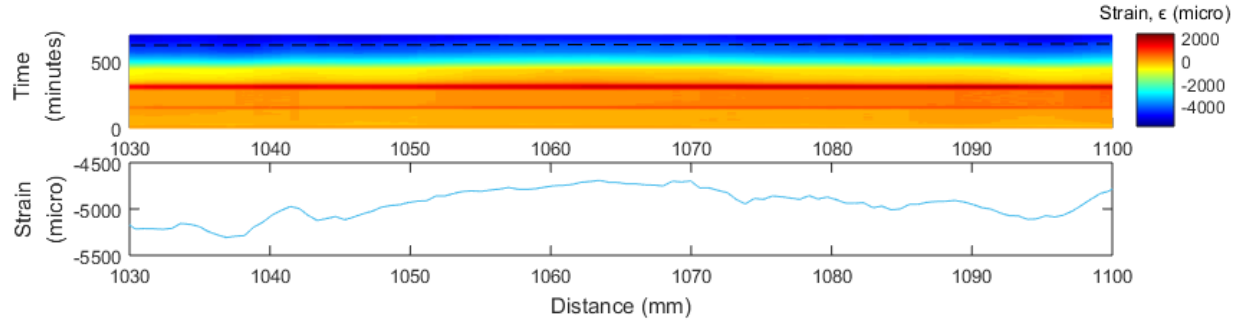

(a)

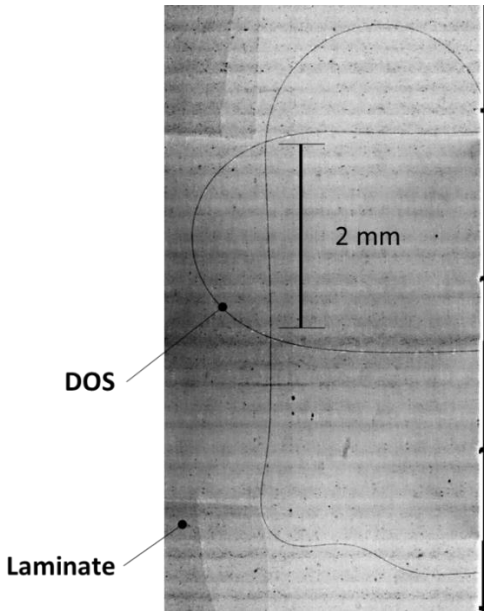

(b)

Figure 8 (a) Mapping residual strain at section C-D in UD; (b) Image of XRD scanning at UD Laminate

Residual strain monitoring 50/40/10 (%0°/% ±45°/%90°) SL

Figure 9 (a) shows the DOS axial strain along regions I, II, and III, which are parallel to the global laminate direction as shown in Figure 2(b) in a SL during the cool-down stage. The level of residual strain is in the range ~(10…-200) $\mu\varepsilon$.

Three inspection lines show the distributed strain sensing at a chosen time instance in three interfaces, [0°/45°], [0°/0°], and [90°/45°] (Figure 9 (b)). A symmetric and balanced laminate should theoretically have no thermal residual bending deformation, i.e. the in-plane laminate strain is expected to be uniform through the laminate thickness. The DOS in different interfaces reports somewhat different strain readings, which are caused by locally variable microstructure of the laminate itself and the resin pockets around the sensor.

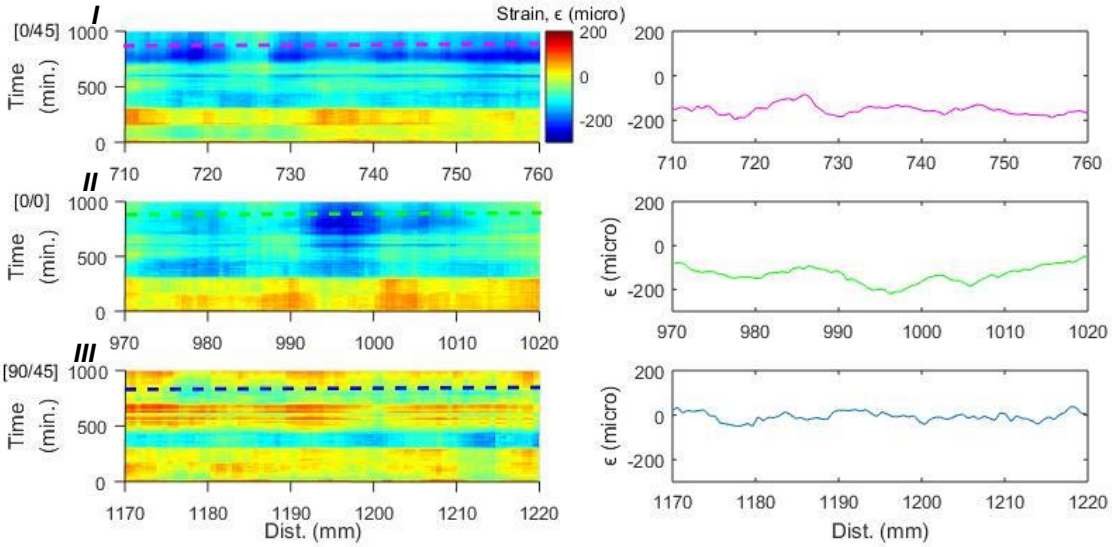

(a) (b)

Figure 9 Mapping residual strain along the path [0°/45°], [0°/0°], and [90°/45°] at SL

Analysis of Transverse Strains from Cure and Thermal Shrinkage in a Unidirectional Laminate (UD)

Figure 10 shows the theoretical transverse strain, ε_{22}, of the UD laminate, with the cure kinetic model, and glass transition model plotted along with the temperature history. The theoretical value was calculated from equation (1) with the input values from equation (3) and (6). The theoretical strain value was calculated when the DoC is above 0.78. As mentioned previously, the DOS reading was overshadowed by the thermal expansion in the transverse direction of the laminate. The calculated chemical shrinkage is approximate 2700 $\mu\varepsilon$ which agrees closely with the experimental result of approximately 2500 $\mu\varepsilon$. During cooling, the epoxy modulus was considered as a function of temperature, as given by equation (4), for calculating the residual strain in equation (1). The theoretical value of the residual strain follows the trend of the experimental value. The final theoretical value for the residual strain is -6200 $\mu\varepsilon$ and the experimental value is in the range of -4800 to -5200 $\mu\varepsilon$ (Figure 8 (a)). This theoretical validation provides confidence that the DOS sensor measurements are in-line with expected results.

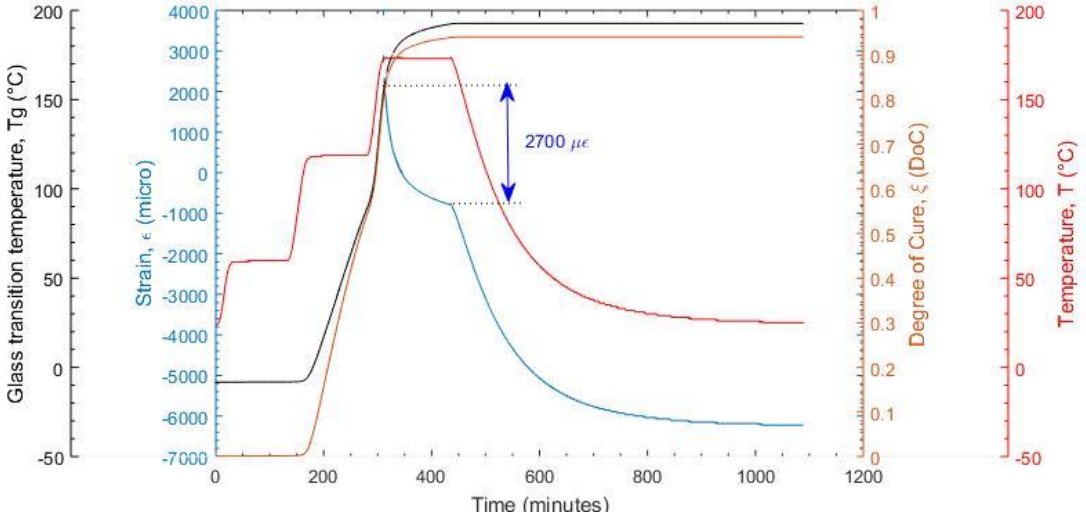

Figure 10 Comparison of Tg, ε_{22} (theoretical), DoC, and with thermal history

Conclusions

The present research utilized the DOS to measure the chemical shrinkage and thermal residual strain in a unidirectional laminate and a structural laminate. The strain measurements provided insight into strain evolution within the laminate behavior at local regions. The cure induced strain was measured in a unidirectional laminate with the DOS, while the analysis of cure kinetics and glass transition temperature evolution allowed for a more accurate interpretation of the experimental measurements. As expected, the axial strain in the UD laminate were small while the transverse strains were much larger due to the low fiber-direction CTE. The cure-induced strains in the structural laminate (SL) were small in all directions as they were constrained by the plies with 0° orientation parallel to the sensor orientation. Due to the small strain and the sensitivity of the measurement system, it is concluded that cure shrinkage cannot accurately be measured by the DOS in a laminate where the ply 0° direction is aligned with the sensor. Also, it is found that the DOS does not adequately capture the cure shrinkage in a UD laminate, because the sensor bonds to the epoxy only when a certain degree of cure is achieved (the sensor cannot measure the material strain before it adheres to the epoxy). In this study, once passing the gelation point (DoC: 0.55), the strain measurements from the DOS were dominated by the thermal expansion of the laminate in the transverse direction. After passing the degree of cure 0.78, the DOS gives a drastic decrease of strain (approximately -2500 $\mu\varepsilon$) signifying the cure shrinkage is partially measured. Lastly, the thermal residual strain was measured by the DOS system. A basic micromechanics approach was applied to simulate the experimental measurement of the UD laminate and validate the measurement technique. The chemical shrinkage and the residual strain from the theoretical calculations showed good agreement with the experimental results providing confidence in using the DOS system for future studies involving strain measurement in composite laminates, with the understanding of the limitations described in this study.

Acknowledgements

The authors would like to thank LUNA Innovations for providing the optical sensors used in this study and the technical support from Dr. Rahim

Bibliography

1. Ramakrishnan, M., et al., *Overview of fiber optic sensor technologies for strain/temperature sensing applications in composite materials.* Sensors (Switzerland), 2016. **16**(1).
2. Di Sante, R., *Fibre Optic Sensors for Structural Health Monitoring of Aircraft Composite Structures: Recent Advances and Applications.* Sensors, 2015. **15**(8): p. 18666.
3. Kinet, D., et al., *Fiber Bragg grating sensors toward structural health monitoring in composite materials: Challenges and solutions.* Sensors (Switzerland), 2014. **14**(4): p. 7394-7419.
4. Kinet, D., et al., *Fiber Bragg Grating Sensors toward Structural Health Monitoring in Composite Materials: Challenges and Solutions.* Sensors, 2014. **14**(4): p. 7394.
5. Bao, X. and L. Chen, *Recent Progress in Distributed Fiber Optic Sensors.* Sensors, 2012. **12**(7): p. 8601.
6. Minakuchi, S., *In situ characterization of direction-dependent cure-induced shrinkage in thermoset composite laminates with fiber-optic sensors embedded in through-thickness and in-plane directions.* Journal of Composite Materials, 2015. **49**(9): p. 1021-1034.
7. Kang, H.K., et al., *Cure monitoring of composite laminates using fiber optic sensors.* Smart Materials and Structures, 2002. **11**(2): p. 279-287.
8. Montanini, R. and L. D'Acquisto, *Simultaneous measurement of temperature and strain in glass fiber/epoxy composites by embedded fiber optic sensors: I. Cure monitoring.* Smart Materials and Structures, 2007. **16**(5): p. 1718.
9. Sánchez, D.M., M. Gresil, and C. Soutis, *Distributed internal strain measurement during composite manufacturing using optical fibre sensors.* Composites Science and Technology, 2015. **120**: p. 49-57.
10. Arhant, M., et al., *Residual Strains using Integrated Continuous Fiber Optic Sensing in Thermoplastic Composites and Structural Health Monitoring.* Experimental Mechanics, 2017.
11. Meadows, L., R.W. Sullivan, and K. Vehorn, *Distributed Optical Sensing in Composite Laminate Adhesive Bonds*, in *57th AIAA/ASCE/AHS/ASC Structures, Structural Dynamics, and Materials Conference*. 2016, American Institute of Aeronautics and Astronautics.
12. Kreger, S.T., et al. *Optical frequency domain reflectometry: Principles and applications in fiber optic sensing*. in *Proceedings of SPIE - The International Society for Optical Engineering*. 2016.
13. Gifford, D.K. and M.E. Froggatt. *Rayleigh scatter based high resolution distributed fiber sensing for safety and security applications*. in *Optics InfoBase Conference Papers*. 2013.
14. Froggatt, M.E. and D.K. Gifford. *Rayleigh backscattering signatures of optical fibers-their properties and applications*. in *Optical Fiber Communication Conference, OFC 2013*. 2013.
15. Bussières, J., et al. *Load monitoring using a rayleigh backscattering fibre optic system*. in *ICAST 2013 - 24th International Conference on Adaptive Structures and Technologies*. 2013.
16. Güemes, A., A. Fernández-López, and B. Soller, *Optical fiber distributed sensing - physical principles and applications.* Structural Health Monitoring, 2010. **9**(3): p. 233-245.
17. Schapery, R.A., *Thermal Expansion Coefficients of Composite Materials Based on Energy Principles.* Journal of Composite Materials, 1968. **2**(3): p. 380-404.
18. Kravchenko, O.G., S.G. Kravchenko, and R.B. Pipes, *Chemical and thermal shrinkage in thermosetting prepreg.* Composites Part A: Applied Science and Manufacturing, 2016. **80**: p. 72-81.
19. Cole, K.C., J.J. Hechler, and D. Noël, *A New Approach to Modeling the Cure Kinetics of Epoxy Amine Thermosetting Resins. 2. Application to a Typical System Based on Bis[4-(diglycidylamino)phenyl]methane and Bis(4-aminophenyl) Sulfone.* Macromolecules, 1991. **24**(11): p. 3098-3110.
20. Kamal, M.R. and S. Sourour, *Kinetics and thermal characterization of thermoset cure.* Polymer Engineering & Science, 1973. **13**(1): p. 59-64.
21. DiBenedetto, A.T., *Prediction of the glass transition temperature of polymers: A model based on the principle of corresponding states.* Journal of Polymer Science Part B: Polymer Physics, 1987.

25(9): p. 1949-1969.
22. Kim, H.-S., S.-H. Yoo, and S.-H. Chang, *In situ monitoring of the strain evolution and curing reaction of composite laminates to reduce the thermal residual stress using FBG sensor and dielectrometry.* Composites Part B: Engineering, 2013. **44**(1): p. 446-452.

Appendix

Cure kinetic model	
Material constants	*value*
$A_1(S^{-1})$	*2.54x10⁴*
E_{A1}*(J/mol)*	*60,628*
m_1	*0.55*
n_1	*21.11*
$A_2(S^{-1})$	*4.84x10⁴*
$E_{A2}(J/mol)$	*61,752*
m_2	*0.8*
n_2	*1.18*
D	*44.3*
ξ_{c0}	*-1.4*
$\xi_{cT}(K^{-1})$	*5.33x10⁻³*

Glass transition temperature model	
Material constants	*value*
T_{g0} (℃)	-8.4
$T_{g\infty}$(℃)	212
λ	0.66

Material constants	*Fiber*
E1f [GPa]	275
E2f [GPa]	15
G12f[GPa]	26
V12f	0.26
V23f	0.26
α_{1f},10^{-6}/℃	-1
α_{2f},10^{-6}/℃	15